Integrating Ultra-Thermal-Sensitive Fluids into Elastomers for Multifunctional Flexible Sensors

*Hanyu Jia, Yonglin He, Xinyue Zhang, Wenbin Du, and Yapei Wang**

The integration of multiple functions is at the forefront of designing electrical devices.[1] Though solid materials have appeared to be the most versatile building blocks for functional purpose,[2–4] the lack of miscibility, self-healing capacity, and flexibility is often encountered when different solid compartments are integrated straightforward. Nowadays, growing interest is paid to liquid materials owing to their several inherent advantages. Generally, liquids have outstanding deformability compared to solids. A little pressure enables the liquids to significantly deform yet maintain their continuity. Liquids also possess unique self-healing ability. Isolated liquids immediately merge together whenever they come in contact. Moreover, liquids are easy to dope or be doped. Many kinds of chemical compounds can be simultaneously dissolved or dispersed into one liquid matrix. Liquid materials in turn are able to flow into solid porous matrix based on capillary force. All these advantages are directing liquid materials to the cutting edge in the development of functional devices.[5–7]

With those attractive features, liquid materials have been adopted in functional devices for several intriguing applications. Concretely, liquids could serve as flexible supporting materials to solve the fracture problems of rigid electrical elements,[8] or build super-slippery surface by filling in porous textured substrates.[9] Liquids could also serve as self-healing conductive materials to facilitate the repair of electrical circuit.[10] However, little is concerned about flexible electronic sensors with the use of liquid materials. Liquids acting as sensing elements are essentially required to own ideal conductivity, appropriate viscosity, and rapid sensing ability. As a class of electrically conducting fluids, ionic liquids (ILs) are good candidates owing to their intrinsic property of electrochemical stability, powerful solubility, negligible volatility, and flame retardancy.[11–13] Till now, rarely has attention been paid to their sensing applications. Here, we find that ionic liquid, 1-ethyl-3-methyl imidazolium acetate, is ultra-thermal sensitive, which rapidly alters its conductivity upon the change of environmental temperature. This particular sensing material satisfies the demands for preparing flexible sensors on the basis of its liquid performance. To realize its full potential, the ionic liquid is integrated into elastomeric resins with rationally designed chambers. The resulting soft sensors have demonstrated advantages of enduring drastic elongation with integrated multiple sensing functions such as thermal, near-infrared (NIR) light, and pressure detection.

As a type of salts in liquid state, ionic liquids act like fluidic semiconductors, becoming more conductive upon the increase of temperature.[14,15] A thorough experimental assessment was paid to the thermal sensitivity of ionic liquids. As shown in **Figure 1**, a typical ionic liquid of 1-ethyl-3-methyl imidazolium acetate ([EMIm][Ac]) was sealed in a glass tube and the fabricated IL sensor was bridged in a circuit to brighten a blue LED. Applied with a low voltage, the LED was not triggered on at room temperature while it lighted up in a few seconds when the glass tube was exposed to a heat gun. Certainly, the LED turned dim if the heat gun was moved away (Figure 1d and Movie S1, Supporting Information). This on–off switch actuated by thermal treatment was attributed to a reversible resistance change of ionic liquid. It is assumed that the mobility of both imidazolium cation and acetate anion was accelerated by the increase of temperature, enabling the ionic liquid to be more conductive. To certify this assumption, three ionic liquids substituted with different alkyl chain on imidazolium cation were employed to assess their ability of thermal response. The ionic liquid with longer chain length shows lower electrical conductivity owing to the decrease of ionic mobility. However, thermal response of ionic liquids is positively related to the chain length at a given temperature difference. When the temperature is increased from 20 to 60 °C, the conductivity change of [OMIm][Ac] with longest chain length could reach as high as 993.4%, exceeding 528.0% of [EMIm][Ac] and 803.5% of [BMIm][Ac] (Figure 1e). The improvement of thermal sensitivity is attributed to the higher phase transition temperature of ionic liquid with longer chain length (see details in Note S1, Supporting Information). It is worth noting that electrical conductivity measured on a conductivity meter (Figure 1f) has a certain relationship with theoretical thermal responses (Figure 1g), which satisfies with a function as below

$$\Delta G/G_0 = \sigma/\sigma_0 - 1 \quad (1)$$

where G_0 and σ_0 are the initial current and conductivity before the sensing test, and σ is the conductivity at a certain temperature. The theoretical thermal response perfectly matches the experimental thermal response, affording great convenience to establish a relationship between temperature and conductivity change.

The ultra-thermal sensitive [OMIm][Ac] could recognize slight temperature change within a body temperature range of 35–45 °C. At the temperature change of 1 °C, the tube-like chip could outcome nearly 10% thermal response (inset of

H. Jia, Y. He, X. Zhang, Prof. Y. Wang
Renmin University of China
Beijing 100872, P.R. China
E-mail: yapeiwang@ruc.edu.cn
Prof. W. Du
State Key Laboratory of Microbial Resources
Institute of Microbiology
Chinese Academy of Sciences
Beijing 100101, P.R. China

DOI: 10.1002/aelm.201500029

ADVANCED ELECTRONIC MATERIALS
www.advelectronicmat.de

Materials Views
www.MaterialsViews.com

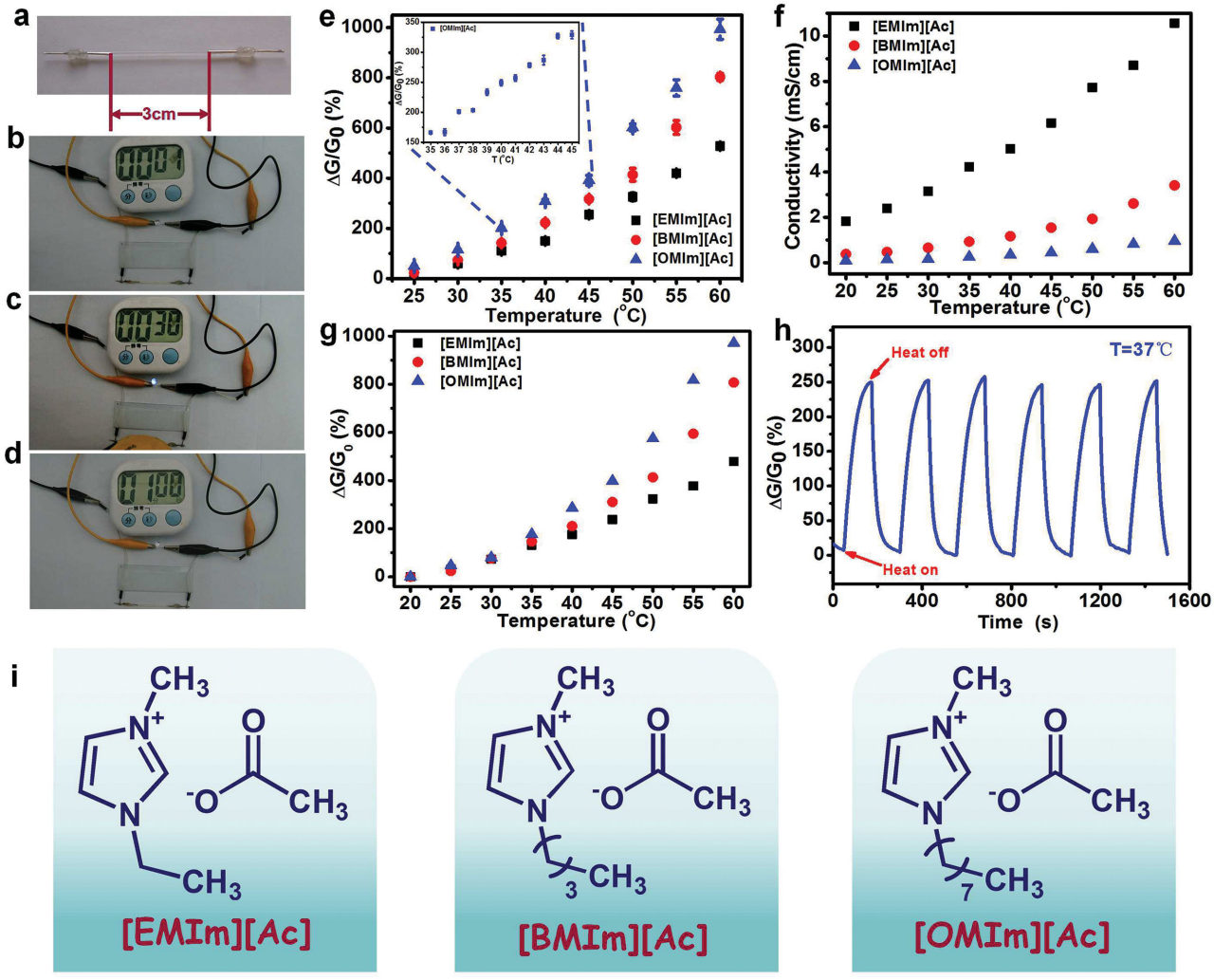

Figure 1. Theoretical study and applications of thermal-sensitive electrical conductivity of ionic liquids. a) Image of a glass chip filled with ionic liquid of [EMIm][Ac], the effective length of the IL chip between two electrodes is 3 cm, both ends of the chip sealed with polypropylene. b–d) Optical images of IL chip bridged in a circuit to regulate the brightness of a blue LED with applied voltage of 3.0 V, the chip heated by heat gun for 30 s b,c) and naturally cooled for 30 s d). e) Thermal response of three ionic liquids, including [EMIm][Ac], [BMIm][Ac], and [OMIm][Ac]. The temperature ranges from 25 to 60 °C with an interval of 5 °C. Room temperature is 20 °C. Inset is the electrical response of [OMIm][Ac] for temperature change ranging from 35 to 45 °C with an interval of 1 °C. f) Measured electrical conductivity of three kinds of ionic liquids at different temperatures. g) Thermal response of three kinds of ionic liquids calculated based on measured electrical conductivity. h) On–off cycles of the thermal response of [OMIm][Ac] chip between 37 °C and room temperature. Error bars represent one standard deviation. i) Molecular structures of three ionic liquids, including [EMIm][Ac], [BMIm][Ac], and [OMIm][Ac].

Figure 1e), offering a great potential for biomedical diagnosis. Notably, the liquid sensing system possesses outstanding sensing stability and reproducibility. The average electrical response of [OMIm][Ac] retains 250% between 37 °C and room temperature (20 °C) under heating and cooling for six cycles (Figure 1h).

Flexible thermal sensors were constructed by integrating ionic liquid into elastomeric substrates. As shown in **Figure 2**, [OMIm][Ac] sealed in a silicone tube shows electrical stability at several bending states, such as knot, line, and ring (Figure 2a). However, the electrical performance is undermined under tensile manipulation. Simultaneous elongation on lateral and constriction on vertical direction caused by tensile strain dramatically increases the resistance of this tube-like sensor. Noting that the change of electrical resistance is stable and reversible (Figure 2c), the strain response may enable the device with function of orientation sensor.[16] The tensile stress yet has side effects on thermal sensing application, hampering the sensor to accurately read out the temperature change. To minimize the unfavorable side effects, a fractal design is introduced in stretchable devices to reduce the change of effective length caused by tensile strain.[17,18] As shown in Figure 2d, we combine a serpentine microchannel within a polydimethylsiloxane (PDMS) template (see Note S2, Figures S2 and S3, Supporting Information, for details). The fractal geometry effectively remains the effective length of liquid circuit invariant, which is of great importance to apply on human skin for collecting clinical information (Figure 2d).[19,20] Consequently, the

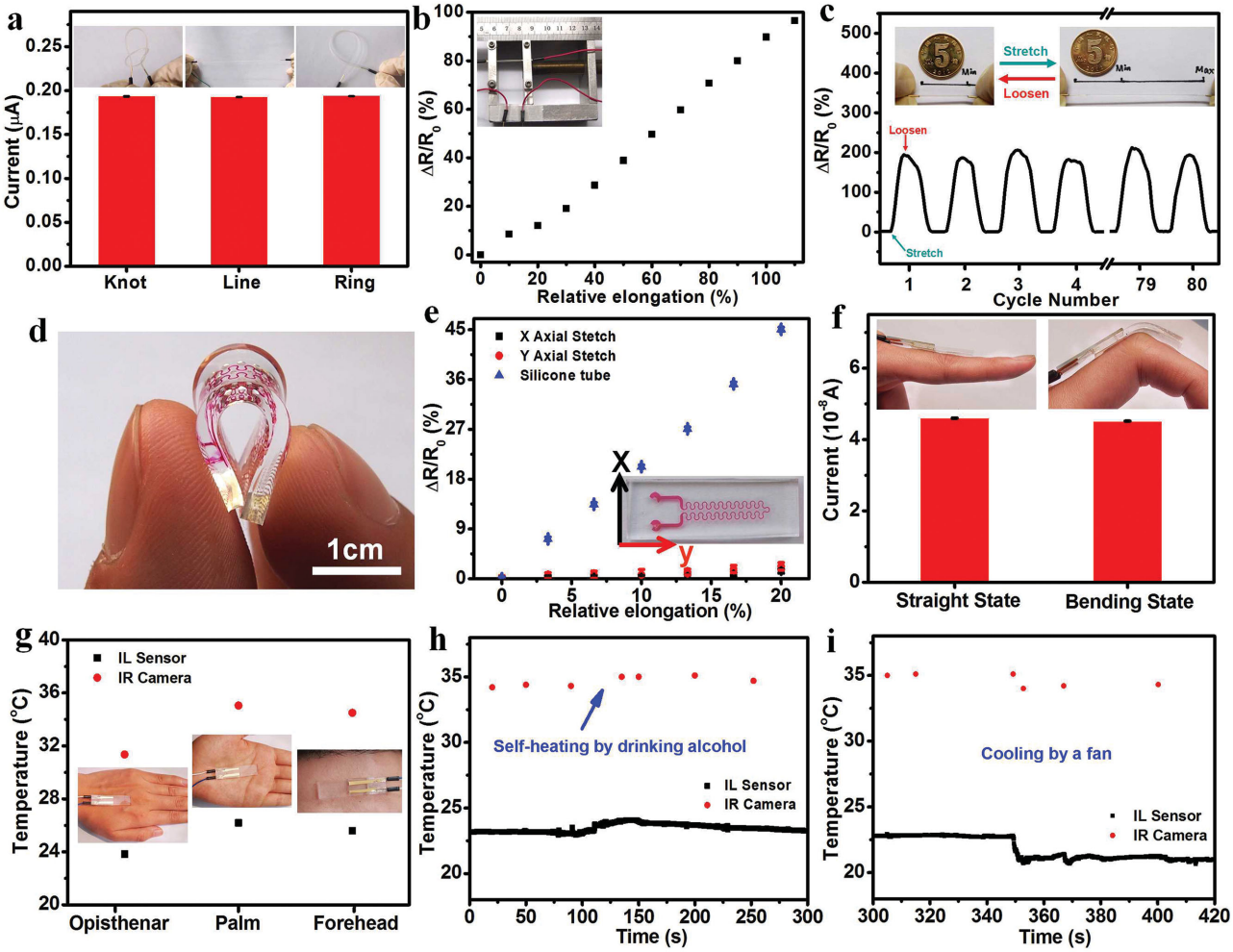

Figure 2. Stretchable sensors with the use of ionic liquid in serpentine microchannel for epidermal temperature characterization. a) The current of [OMIm][Ac] tube with three different wrapping pattern under voltage of 1.0 V, including knot (left inset), line (middle inset), and ring (right inset). b) Stress response of the flexible silicone tube filled with [OMIm][Ac] under different tensile states. Inset is a photograph of experimental setup of stress tests. The initial length is 2.0 cm. c) Stress response of [OMIm][Ac] tube for 80 stretch–loosen cycles. Inset photographs show the different states of the flexible tube. d) Photograph of a stretchable sensing device with serpentine microchannel. The device was filled with rhodamine aqueous solution to highlight the serpentine microchannel. e) Stress response of normal silicone tube and stretchable device with two vertical orientations under different tensile states. The orientation of X axial and Y axial are shown in the inset photograph. The initial length of silicone tube is 15.0 cm. f) Current of stretchable device in bending state and straight state, with applied voltage of 1.0 V. Insets are photographs of stretchable device sticking on the finger knuckle with straight and bending state. g) Various parts of body temperatures measured by IL sensor (black point) and IR camera (red point), including opisthenar, palm, and forehead, as shown in inset photographs. Real-time monitoring of body temperature on forehead by IR camera and IL sensor after drinking alcohol for dozens of minutes h) and cooling by a fan i).

relative resistance changes of [OMIm][Ac] stretched on two vertical directions, including X axial and Y axial, are both no more than 2.2%, compared with 45.1% of silicone tube at the same stretching degree of 20% (Figure 2e). An exemplary application shows that the IL sensor mounted on finger knuckle at straight state and bending state exhibits excellent property of flexibility (Figure 2f).

A relationship between temperature (T) and thermal response ($\Delta G/G_0$) is established to identify the real-time temperature based on the electrical readout. Applied temperature and electrical conductivity of ionic liquids obey Equation (2) as shown below, which is a Vogel–Tamman–Fulcher (VTF) type equation[21]

$$\sigma(T) = \sigma_\infty \exp\left(-B/(T - T_v)\right) \quad (2)$$

where $\sigma(T)$ is the electrical conductivity of [OMIm][Ac] at a certain temperature T, other factors including σ_∞, B, and T_v are constants. The conductivity change as function of temperature perfectly fits Equation (2) (Figure S1, Supporting Information). Combing Equation (1) with Equation (3), the temperature is relevant to the conductivity change ($\Delta G/G_0$) as follows

$$T = T_v - \frac{B}{\ln\left(H \times \left(1 + \Delta G/G_0\right)\right)} \quad (3)$$

ADVANCED ELECTRONIC MATERIALS
www.advelectronicmat.de

www.MaterialsViews.com

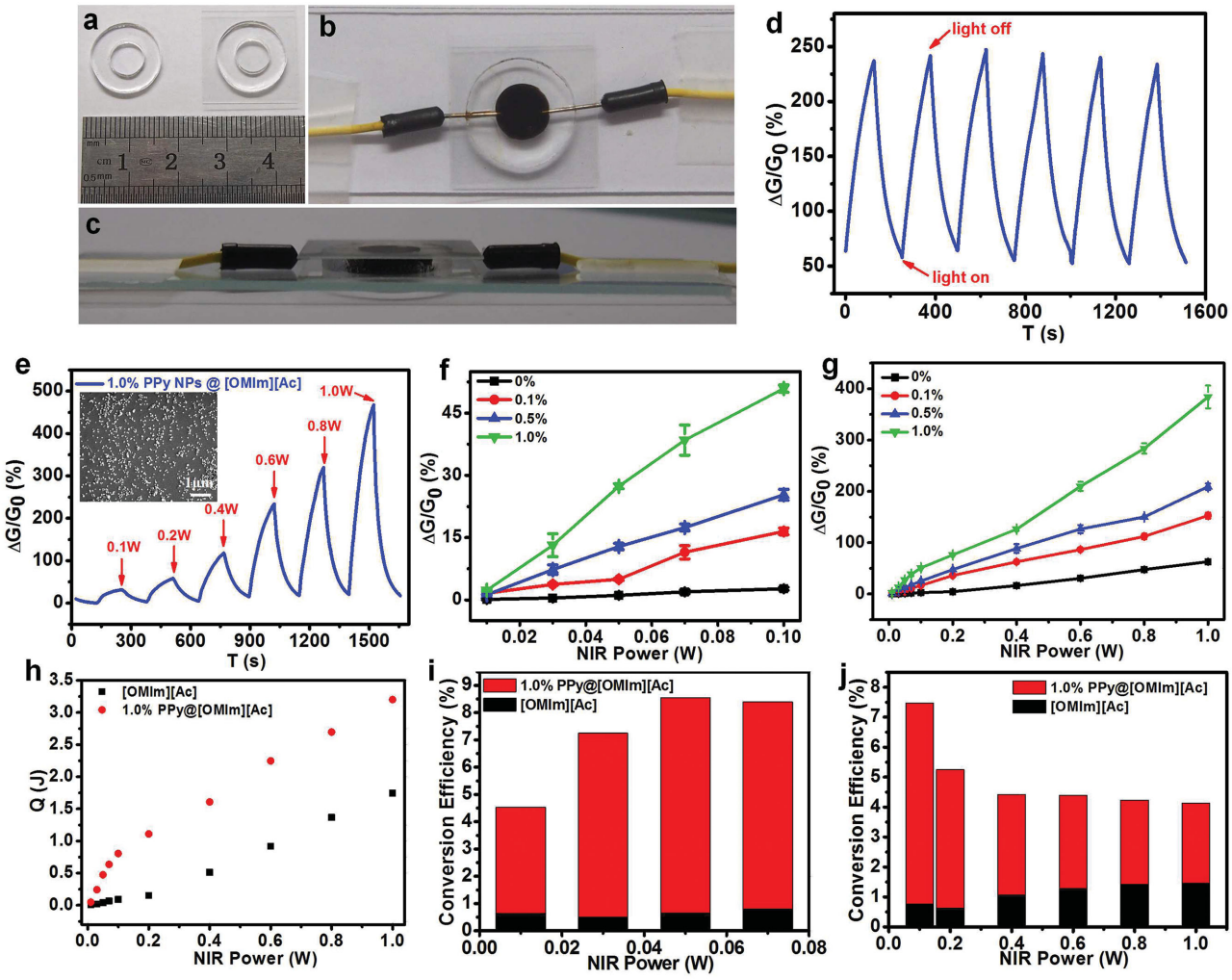

Figure 3. NIR sensing behaviors of IL sensor with the cooperation of polypyrrole nanoparticles. a) Photograph of a PDMS chamber (left) and sealed with cover glass on both sides (right). Effective sensing area is 0.5 cm^2. The photographs of IL sensor doping with polypyrrole NPs on top view b) and side view c). d) On–off cycles of NIR (808 nm) responses of an IL sensor doping with 1.0 wt% PPy NPs, NIR power is 0.5 W. e) On–off cycles of NIR responses of IL sensor for six NIR power, ranging from 0.1 to 1.0 W. Inset is the SEM image of PPy NPs. f,g) NIR responses of IL sensors doping with different quantity of PPy NPs, including weight ratio of 0%, 0.1%, 0.5%, and 1.0%, for different power of NIR ranging from 0.01 to 1.0 W. h) The heat resulting from photothermal conversion of IL sensors doped with or without PPy NPs at different NIR power. i,j) Photothermal conversion efficiency of IL sensors doped with or without PPy NPs at different NIR power.

$$H = \sigma_0/\sigma_\infty \quad (4)$$

To be specific, H represents the ratio of the initial conductivity (σ_0) before thermal treatments and theoretical conductivity (σ_∞) at high temperature limit. According to the VTF equation, body temperature, for instance, on opisthenar, palm, or forehead could be readily estimated through thermal response of ionic liquid sensor (Figure 2g). Temperature determined by the sensor well matches the result read on IR camera with a coefficient compensated. In addition to characterizing the local temperature of human body, the flexible sensor can also monitor the slight change of body temperature onsite. As shown in Figure S4, Supporting Information, a sensor was adhered to the forehead of a male volunteer to monitor his temperature variation. After drinking a certain amount of alcohol (t = 0–10 s), the volunteer self-heated (t = 10–300 s), and was cooled by a fan (t = 348–352 s). Abrupt temperature change at t = 110–130 and 348–352 s was distinguished electrically by IL sensor or optically by IR camera (Figure 2h,i).

Doping functional materials into ionic liquids extends the electrical device for more potential. Herein, we loaded a dark material of polypyrrole nanoparticles with capability of photothermal conversion in the ionic liquid of [OMIm][Ac] intending to prepare NIR sensors. The polypyrrole nanoparticles (PPy NPs) with an average size of 28 nm (Figure S6, Supporting Information) were polymerized from pyrrole through a microemulsion method, using ferric chloride as the oxidant and polyvinyl alcohol as the emulsifier. As shown in **Figure 3**a and Figure S5, Supporting Information, an integrated NIR sensing device is constructed by a PDMS chamber sealed with glass covers. Ionic liquid doped with PPy NPs was injected into the chamber which was connected into a circuit for fulfilling NIR sensing tests. Polypyrrole is able to convert NIR energy to

heat.[22] As such, NIR irradiation can trigger electrical response of the device on the basis of thermal excitation effect. Analogue to thermal response, the conductivity was increased immediately upon exposure to NIR light. A reproducible on–off response was achieved by turning the light on and off alternatively (Figure 3d). The conductivity change was positively correlated with the dose of NIR irradiation. The doping amount of PPy NPs also has positive effect to NIR sensing ability of the ionic liquid sensor (Figure 3f,g). A significant conductivity change (384.0%) is reached if 1.0 wt% PPy NPs were dosed at a given light power (1.0 W), much higher than 209.0% and 152.9% of ionic liquid doping with 0.5 and 0.1 wt% PPy NPs, respectively. Moreover, light with ultralow power (0.01 W) that can be generated on the light resource in our lab was successfully sensitized by the ionic liquid loading 1.0 wt% PPy NPs. The theoretical detection limit was estimated by analyzing a sensing curve irradiated with 0.05 W NIR light, with 100 consecutive points randomly selected to calculate the standard deviation (SD).[23] DL varies with the SD of blank values and the average peak height (APH), DL = 3SD×0.05/APH. A detection limit of 9.25×10^{-4} W was estimated. Noting that the polyvinyl alcohol on nanoparticle surface may have hydrogen-bonding interaction with ionic liquid, PPy NPs were well dispersed in ionic liquid and there was no precipitation in the elastomeric chamber without touching the device for a half year. In comparison with the paper NIR sensor with the use of conducting polymer,[22] both flexibility and sensitivity were dramatically improved with the combination of ionic liquid and conducting materials.

The contribution of PPy NPs to NIR detection was quantified by the evaluation of photothermal conversion efficiency (η) of ionic liquid with or without loading PPy NPs. Specifically, the efficiency meets Equation (5) as follows, where Q is the Joule heat of ionic liquid, E and P refer to the total photo energy and power of the NIR laser, respectively. The heat energy (Q) is defined by the specific heat (C_p (T)), temperature (T), and mass (m) of doped ionic liquid

$$\eta = \frac{Q}{E} = \frac{Q}{P \times t} \tag{5}$$

$$Q = m\int_{T_0}^{T} C_P(T)\,\mathrm{d}T \tag{6}$$

The specific heats of neat ionic liquid and ionic liquid doped with 1.0% PPy NPs were estimated as a function of temperature through the method of differential scanning calorimetry (DSC), with 100 consecutive points selected to calculate the relationship between specific heat with temperature, which is shown as follows

$$C_P(T) = A_0 + A_1T + A_2T^2 \tag{7}$$

where A_0, A_1, and A_2 are constants that are calculated through the DSC results. Quadratic functions were obtained with a fitting degree of 99.75% (neat ionic liquid) and 96.45% (ionic liquid doped with PPy NPs), respectively (Figure S8, Supporting Information). The Joule heat evolution from NIR light was extremely improved with the aid of PPy NPs (Figure 3h). At low irradiation power ranging from 0.01 to 0.10 W, the Joule heat produced in ionic liquid is mainly contributed by the photothermal conversion of PPy NPs. The ionic liquid has negligible capability of photothermal conversion in comparison with PPy NPs. For example, the energy conversion efficiency of doped ionic liquid reached 7.89% than 0.66% of pure ionic liquid at a given light power of 0.05 W. However, the conversion efficiency is not further improved when NIR light with stronger power is applied. Regarding that the heat energy based on photothermal conversion by PPy NPs already reaches maximum, thermal effect by light excitation becomes predominated to the Joule heat.

The ionic liquid could not only serve as a host material to dope with functional agents, but also act as a guest material to be doped into porous scaffolds for inherent applications.[24,25] With the properties of inert, nontoxic, nonflammable, and highly flexible, a porous PDMS sponge is prepared as the 3D scaffold to load with ionic liquid.[26–29] The PDMS sponge is able to adsorb [OMIm][Ac] quickly owing to the capillary force given by its porous morphology. The PDMS sponge filled with ionic liquid was bridged into a circuit to monitor its electrical response to external stimuli. In addition to thermal responsive performance, the sponge is able to feel the pressure on it. The electrical conductivity increases under pressure and recovers with the removal of pressure (**Figure 4**a). The pressure sensing is attributed to the change of volume fraction of ionic liquid in the PDMS sponge. It is assumed that air is extruded when the sponge is compressed, increasing the volume fraction of ionic liquid, that more electrical pathways are connected to improve the electrical conductivity.[30,31]

There are two factors influencing the pressure sensitivity of PDMS sponge,[32] including the crosslinking degree of PDMS and the volume fraction of ionic liquid in sponge. The crosslinking degree determines the compressive deformation under a given pressure. Three types of PDMS sponges with different crosslinking degrees were prepared by changing the weight ratio of precursor and curing agent as 10:1, 15:1, and 20:1. Notably, PDMS sponge with lower crosslinking degree has a greater deformation under fixed forces, exhibiting more sensitive pressure response (Figure 4b). It is noteworthy that the PDMS sponge responds quickly to the pressure. The conductivity change is almost synchronous with the pressure change through the pressure gauge (Figure 4e). The volume fraction of ionic liquid in the sponge also offers extraordinary control of the pressure sensitivity. In addition, lower crosslinking degree endows the PDMS sponge with higher pressure sensitivity, however, limits the measurements in a narrow pressure range (Figure 4d). The conductivity change is raised first and then decreased upon the increase of the volume fraction (Figure 4c). Regardless of conductivity of PDMS, the electrical performance relies on the number of conductive pathways in the porous sponge. The filled air cuts the conductive pathway while it is essentially needed to induce the change of pathway number under pressure. Therefore, a maximum conductivity change has to be reached at an appropriate volume fraction, e.g., 11.68% if applied with a force of 0.5 N.

To realize its full potential, simultaneous sensing detection of pressure and temperature is coming into focus.[33,34] The

ADVANCED ELECTRONIC MATERIALS
www.advelectronicmat.de

Materials Views
www.MaterialsViews.com

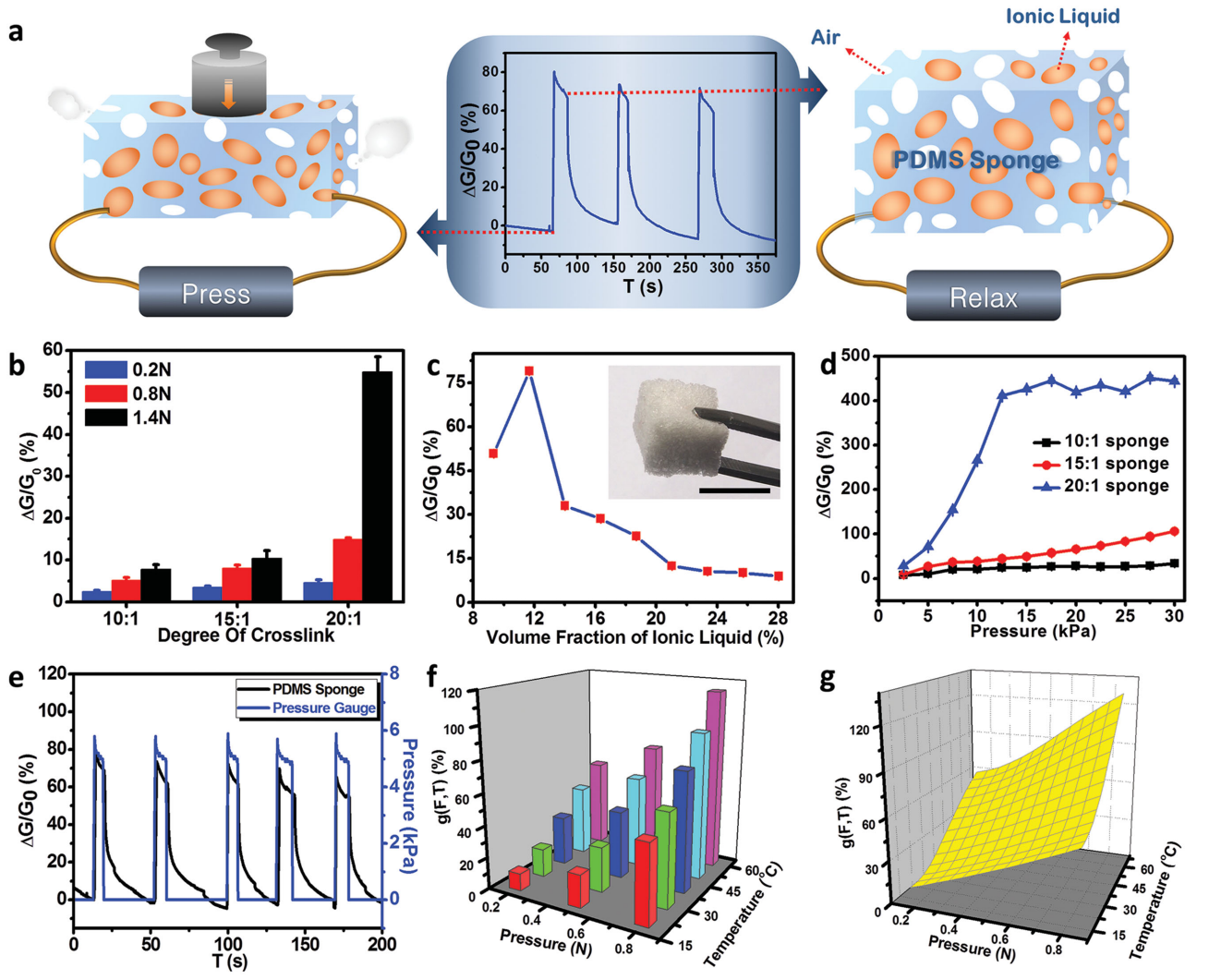

Figure 4. Pressure sensing behaviors of ionic liquid sensor and theoretical signal separation for temperature and pressure responses. a) Schematic illustration of the pressure sensing principle of PDMS sponge filled with ionic liquid of [OMIm][Ac]. Inset figure shows the time of applied pressure force and relaxation. b) Different pressure sensing tests of PDMS sponge with three crosslinking degrees, including 10:1, 15:1, and 20:1. The bearing area of PDMS sponge was fixed as 1.0 cm^2. c) The optimized volume fraction of ionic liquid to sense pressure of 0.5 N with the highest sensitivity. Inset is the photograph of a PDMS sponge, scale bar is 1 cm. d) Pressure sensing tests of PDMS sponge with different crosslinking degrees. The pressure ranges from 0.25 to 3.00 N with an interval of 0.25 N. e) The pressure responses measured by PDMS sponge, compared with the calibrated pressure determined by a standard pressure gauge under applying a same pressure of 0.5 N for five cycles. f) The real mixing responses of PDMS sponge for sensing different temperatures and pressures simultaneously. The tested pressures were selected as 0.2, 0.5, and 0.8 N, respectively. The tested temperatures were selected as 20, 30, 40, 50, and 60 °C, respectively. g) Theoretical simulation of mixing responses for signal separation into pressure and temperature.

remarkable difference of sensing time between pressure (less than 1 s) and temperature (over 120 s) renders the possibility to read and distinguish two signals by the sponge loading with ionic liquid. Two signals in a typical sensing curve can be divided into a pressure response (f_B (F)) and a mixing response consisting of the temperature response and pressure response (ϕ (F, T)), respectively

$$g(F,T) = f_B(F) + \varphi(F,T) \tag{8}$$

$$f_B(F) = d \times F^2 + h \times F \tag{9}$$

$$\varphi(F,T) = a \times e^{\frac{b}{T+c}} \tag{10}$$

d and h in the function of f_B (F) are defined as 13.34 and 50.66 by the analysis of Figure 4d. The parameters of a, b, and c are the function of pressure force (F) (noted in Note S4, Supporting Information). As a consequence, a 3D diagram of g (F, T) is simulated in Figure 4g, which precisely matches the test result (Figure 4f). To further certify the availability of sensing function, a random sensing curve was analyzed, obtaining temperature and pressure that satisfy the real values (Figure S13 and Note S4, Supporting Information).

In summary, we have represented a paradigm for integrating ultra-thermal sensitive ionic liquid into elastomeric scaffolds, opening new opportunities in sensing applications. The fluidic nature of ionic liquid combined with its ease of doping leads to the creation of numerous flexible sensors. Typical thermal sensor not only possesses ultra-high sensitivity but also offers an attractive solution to eliminate the fracture under tensile stress. Ionic liquid could be readily modified with the use of dark materials for fulfilling the test of NIR light. Taking into account the merits of NIR light, this particular light sensor is believed valuable for remote operation. Though the sensor is still at laboratory level, it has shown temperature and pressure information could be gathered and distinguished. We believe that ionic liquids will become a class of star materials in the vast production of high-level optoelectronics and sensors owing to its intrinsic simplicity and generality. Taking advantage of its fluidic performance, we may consider flowing ionic liquids into targeting place and spatially assemble biological sensors in tissues. Moreover, the integration of multiple functions will be concerned by isolating or fusing ionic liquid within many other materials.

Supporting Information

Supporting Information is available from the Wiley Online Library or from the author.

Acknowledgements

This work was financially supported by the National Natural Science Foundation of China (51373197, 21422407), Trans-Century Training Programme Foundation for the Talents by the State Education Commission (NCET-12-0530).

Received: January 16, 2015
Revised: January 25, 2015
Published online: February 23, 2015

[1] G. R. Whittell, I. Manners, *Adv. Mater.* **2007**, *19*, 3439.
[2] P. Avouris, Z. Chen, V. Perebeinos, *Nat. Nanotechnol.* **2007**, *2*, 605.
[3] Q. Qian, J. Wang, F. Yan, Y. Wang, *Angew. Chem. Int. Ed.* **2014**, *53*, 4465.
[4] A. J. Heeger, *Semiconducting and Metallic Polymer*, Oxford University Press, Oxford **2010**.
[5] L. Dong, A. K. Agarwal, D. J. Beebe, H. Jiang, *Nature* **2006**, *442*, 551.
[6] C. Ohm, M. Brehmer, R. Zentel, *Adv. Mater.* **2010**, *22*, 3366.
[7] H. J. Snaith, L. Schmidt-Mende, *Adv. Mater.* **2007**, *19*, 3187.
[8] S. Xu, Y. Zhang, L. Jia, K. E. Mathewson, K. I. Jang, J. Kim, H. Fu, X. Huang, P. Chava, R. Wang, S. Bhole, L. Wang, Y. J. Na, Y. Guan, M. Flavin, Z. Han, Y. Huang, J. A. Rogers, *Science* **2014**, *344*, 70.
[9] T.-S. Wong, S. H. Kang, S. K. Y. Tang, E. J. Smythe, B. D. Hatten, A. Grinthal, J. Aizenberg, *Nature* **2011**, *477*, 437.
[10] E. Palleau, S. Reece, S. C. Desai, M. E. Smith, M. D. Dickey, *Adv. Mater.* **2013**, *25*, 1589.
[11] M. Armand, F. Endres, D. R. MacFarlane, H. Ohno, B. Scrosati, *Nat. Mater.* **2009**, *8*, 621.
[12] R. D. Rogers, K. R. Seddon, *Science* **2003**, *302*, 792.
[13] T. Torimoto, T. Tsuda, K. Okazaki, S. Kuwabata, *Adv. Mater.* **2010**, *22*, 1196.
[14] J. Vila, P. Gines, J. M. Pico, C. Franjo, E. Jimenez, L. M. Varela, O. Cabeza, *Fluid Phase Equilib.* **2006**, *242*, 141.
[15] H. Tokuda, S. Tsuzuki, M. A. B. H. Susan, K. Hayamizu, M. Wantanabe, *J. Phys. Chem. B* **2006**, *110*, 19593.
[16] L. Persano, C. Dagdeviren, Y. Su, Y. Zhang, S. Girardo, D. Pisignano, Y. Huang, J. A. Rogers, *Nat. Commun.* **2013**, *4*, 1633.
[17] J. A. Fan, W.-H. Yeo, Y. Su, Y. Hattori, W. Lee, S.-Y. Jung, Y. Zhang, Z. Liu, H. Cheng, L. Falgout, M. Bajema, T. Coleman, D. Gregoire, R. J. Larsen, Y. Huang, J. A. Rogers, *Nat. Commun.* **2014**, *5*, 3266.
[18] J. A. Rogers, T. Someya, Y. Huang, *Science* **2010**, *327*, 1603.
[19] R. C. Webb, A. P. Bonifas, A. Behnaz, Y. Zhang, K. J. Yu, H. Cheng, M. Shi, Z. Bian, Z. Liu, Y.-S. Kim, W.-H. Yeo, J. S. Park, J. Song, Y. Li, Y. Huang, A. M. Gorbach, J. A. Rogers, *Nat. Mater.* **2013**, *12*, 938.
[20] M. L. Hammock, A. Chortos, B. C.-K. Tee, J. B.-H. Tok, Z. Bao, *Adv. Mater.* **2013**, *25*, 5997.
[21] J. Leys, R. N. Rajesh, P. C. Menon, C. Glorieux, S. Longuemart, P. Nochemann, M. Pallens, K. Binnemans, *J. Chem. Phys.* **2010**, *133*, 034503.
[22] H. Jia, J. Wang, X. Zhang, Y. Wang, *ACS Macro Lett.* **2014**, *3*, 86.
[23] J. Wang, X. Zhang, X. Huang, S. Wang, Q. Qian, W. Du, Y. Wang, *Small* **2013**, *9*, 3759.
[24] C.-Y. Wu, W.-H. Liao, Y.-C. Tung, *Lab Chip* **2011**, *11*, 1740.
[25] B. Nie, R. Li, J. D. Brandt, T. Pan, *Lab Chip* **2014**, *14*, 1107.
[26] S.-J. Choi, T.-H. Kwon, H. Im, D.-I. Moon, D. J. Baek, M.-L. Seol, J. P. Duarte, Y.-K. Choi, *Appl. Mater. Interfaces* **2011**, *3*, 4552.
[27] R. Li, B. Nie, P. Digiglio, T. Pan, *Adv. Funct. Mater.* **2014**, *24*, 6195.
[28] J.-B. Chossat, Y.-L. Park, R. J. Wood, V. Duchaine, *IEEE Sens. J.* **2013**, *13*, 3405.
[29] Y.-L. Park, C. Majidi, R. Kramer, P. Bérard, R. J. Wood, *J. Micromech. Microeng.* **2010**, *20*, 125029.
[30] L. Pan, A. Chortos, G. Yu, Y. Wang, S. Isaacson, R. Allen, Y. Shi, R. Dauskardt, Z. Bao, *Nat. Commun.* **2014**, *5*, 3002.
[31] C. Pang, G.-Y. Lee, T.-I. Kim, S. M. Kim, H. N. Kim, S.-H. Ahn, K.-Y. Suh, *Nat. Mater.* **2012**, *11*, 795.
[32] S. C. B. Mannsfeld, B. C.-K. Tee, R. M. Stoltenberg, C. V. H.-H. Chen, S. Barman, B. V. O. Muir, A. N. Sokolov, C. Reese, Z. Bao, *Nat. Mater.* **2010**, *9*, 859.
[33] N. T. Tien, S. Jeon, D.-I. Kim, T. Q. Trung, M. Jang, B.-U. Hwang, K.-E. Byun, J. Bae, E. Lee, J. B.-H. Tok, Z. Bao, N.-E. Lee, J.-J. Park, *Adv. Mater.* **2014**, *26*, 796.
[34] C. Hou, H. Wang, Q. Zhang, Y. Li, M. Zhu, *Adv. Mater.* **2014**, *26*, 5018.

